Neoclassical transport processes in weakly collisional plasmas with fractured velocity distribution functions

A.A. KABANTSEV,[1] C.F. DRISCOLL,[1] D.H.E. DUBIN[1]
and Y.A. TSIDULKO[2]

[1]University of California at San Diego, La Jolla, CA 92093, USA
[2]Budker Institute of Nuclear Physics, Novosibirsk 630090, Russian Federation

Abstract. Ripples in magnetic or electrostatic confinement fields give rise to trapping separatrices, and conventional neoclassical transport theory describes the *collisional* trapping/detrapping of particles with fractured distribution function. Our experiments and novel theory have now characterized a new kind of neoclassical transport processes arising from *chaotic* (nominally collisionless) separatrix crossings, which occur due to *E*×*B* plasma rotation along *θ–ruffled* or wave-perturbed separatrices. This *chaotic* neoclassical transport becomes dominant at low collisionality when the collisional spreading of particle energy during the dynamical period is less than the separatrix energy ruffle.
PACS: 52.25.Fi, 52.27.Aj

1. Introduction

All laboratory devices for plasma confinement have some level of trapping separatrices, arising from variations in magnetic field strength and external potentials. The locally-trapped and passing populations of particles may then have significantly different drift orbits, (so called *neoclassical effects*), giving rise to large dissipative dynamical steps when separatrix crossings occur. Neoclassical transport (NCT) theory analyzes the particle transport and wave damping effects arising from *collisional* scattering (at rate ν) across a rigidly uniform separatrix in a variety of geometries [1-4], and experimental corroboration has been obtained in some regimes of a moderate collisionality [5, 6].

Here, we describe the enhanced transport which occurs when the ripple separatrix is itself *ruffled* in the (θ) direction of plasma drift, or when the separatrix fluctuates due to presence of waves/turbulence in the plasma. In such cases the drifting particles see a time-varying separatrix barrier, and they can *chaotically* transit between locally-trapped and passing orbits near the separatrix. As a result, the NCT rate does not depend directly on the collision frequency. However, collisions are still important here in the sense that their stochastic input has to be strong enough for a particle performing its next separatrix crossing to "forget" about the previous one (making consecutive crossings statistically independent).

In our experiments with θ–ruffled separatrices, these chaotic crossings lead to considerably enhanced neoclassical ripple transport driven by a global magnetic tilt asymmetry. The experiments utilize externally controlled electrostatic ruffles or fluctuations on the separatrix, and can thus identify the novel *chaotic* neoclassical ripple transport scaling as $\nu^0 B^{-1}$, and thus distinct from *collisional* neoclassical ripple transport scaling as $\nu^{1/2} B^{-1/2}$.

This chaotic transport mechanism can substantially modify particle transport in low collisionality regimes associated with fusion plasmas, though it has previously been considered to be ineffective due to a presumed symmetry of such transitions [7]. Indeed, one should realistically expect strong transport even with near-zero collisionality.

2. Experimental setup

The experiments utilize a cylindrical Penning-Malmberg trap to confine quiescent, low-collisionality pure electron plasmas [8-10]. Electrons are confined radially by a nominally uniform axial magnetic field $B\hat{z}$, with $0.04 \le B \le 2\,\mathrm{T}$; and are confined axially by voltages $V_c = -100\,\mathrm{V}$ on end cylinders of radius $R_W = 3.5\,\mathrm{cm}$. The electron columns have length $L \approx 49\,\mathrm{cm}$, and radial density profile $n(r)$ with central density $n_0 \approx 1.6\times10^7\,\mathrm{cm}^{-3}$ and line density $N_L = \pi R_p^2 n_0 \approx 6.1\times10^7\,\mathrm{cm}^{-1}$. The unneutralized charge results in an equilibrium potential energy $\phi_e(r)$ with $\phi_{e0} \approx +28\,\mathrm{eV}$ at $r = 0$ (here, all ϕ's are in energy units). This gives an *E*×*B* rotation frequency $f_E(r)$ which decreases monotonically from $f_{E0} \approx 230\,\mathrm{kHz}\times(B/1\mathrm{kG})^{-1}$. The bulk electrons have a near-Maxwellian velocity distribution $F_M(E)$ with thermal energy $T \lesssim 1\mathrm{eV}$, giving axial bounce frequency $f_b \equiv \bar{\upsilon}/2L \approx 430\,\mathrm{kHz}$ and rigidity parameter $\mathcal{R} \equiv f_b / f_E \approx 2\times(B/1\mathrm{kG})$. Experiments are done in ultrahigh vacuum having a base pressure of $\sim 10^{-10}$ torr, so the electron-neutral collision rate $\nu_{eN} \sim 0.1/\mathrm{sec}$ is negligible in comparison with electron-electron collision rate $\nu \sim 100/\mathrm{sec}$.

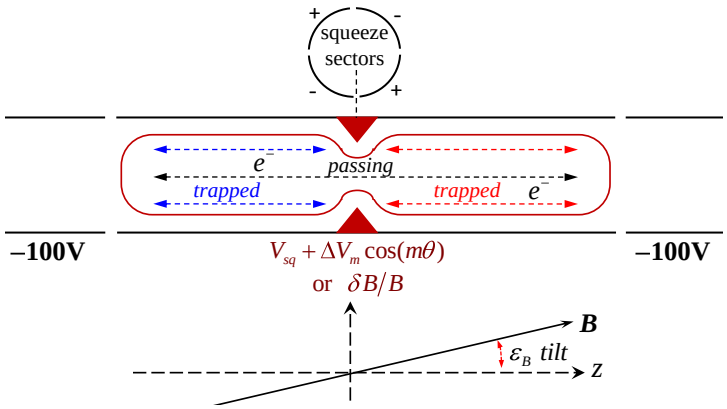

Figure 1. Schematic of electron plasma with tilt ε_B and a trapping barrier in a cylindrical Penning-Malmberg trap.

An electrostatic trapping barrier (separatrix) $\phi_s(r,\theta)$ is created by a "squeeze" wall voltage V_{sq} (see Fig.1). Here, we include the effects of adjustable θ-sector (ruffles) voltages $\pm\Delta V_m$, giving controllable interior separatrix energy $\phi_s(r,\theta) = \phi_{s0}(r) + \Delta\phi_m \cos[m(\theta - \theta_m)]$. Here we focus mostly on $m = 2$ ruffles, created by voltages $\pm\Delta V_2$ applied to four 60° sectors, extending over $\Delta z = 4\,\mathrm{cm}$ near the $z = 0$ center. At every plasma radius, low energy particles are trapped in either the left or right end, whereas higher energy passing particles transit the entire length of the column. Ruffles spread the characteristic separatrix energy by $\Delta\phi_m(r) \sim \Delta V_m (r/R_W)^m$, somewhat reduced by plasma shielding.

Particles change from ripple trapped to passing (and vice versa) due to binary collisions at rate ν, due to drift-rotation across θ-ruffle variations $\Delta\phi_m$, or due to temporal fluctuations $\Delta\phi(t)$ in the separatrix energy. The electron-electron collisionality in the present experiments is relatively low $(\nu \sim 100/\mathrm{sec})$, and collisions acting for a drift-rotation period spread the separatrix by an energy width $\Delta W_c \equiv T(\nu/2\pi f_E)^{1/2}(\phi_{s0}/T)^{1/2} \approx 0.02\,\mathrm{eV} \times (B/1\mathrm{kG})^{1/2}$. Thus, the chaotic (de)trapping processes will be important when $\Delta\phi_m(r) \geq \Delta W_c$, or when $\Delta\phi(t) \geq \Delta W_c$.

We diagnose the bulk radial expansion of the plasmas, characterized by the mean-square radius $\langle r^2 \rangle \equiv \int 2\pi r dr\, r^2 n(r)$ and the overall expansion rate $\nu_{<r^2>}$ defined as

$$\nu_{<r^2>} \equiv \frac{1}{\langle r^2 \rangle} \frac{d\langle r^2 \rangle}{dt}. \tag{1.1}$$

Fortunately, $\nu_{<r^2>}$ can be accurately and readily obtained from the continuously measured frequency $f_2(t)$ of a small amplitude $m = 2$ diocotron mode, as $\nu_{<r^2>} = (1/f_2)df_2/dt$. The bulk expansion rate $\nu_{<r^2>}$ is an integral measure of the full radial flux that includes both mobility and diffusive contributions, both being proportional to the radial diffusion coefficient $D_r(r)$.

3. Neoclassical transport from collisional and chaotic separatrix steps

Radial particle transport is conveniently driven by a global magnetic tilt asymmetry $B_\perp$ with controlled magnitude $\varepsilon_B \equiv B_\perp / B_z \leq 0.001$ and chosen tilt direction $\theta_B \equiv \tan^{-1}(B_y/B_z)$ (thus, rotated by $\alpha \equiv \theta_B - \theta_m$ relative to the ruffle). This tilt is equivalent to applying z-antisymmetric wall voltages $V_a(R_W,\theta,z) = \varepsilon_B z(2eN_L/R_W)\cos(\theta - \theta_B)$, which causes interior Debye-shielded z-asymmetric potentials $\delta\phi_a(r,z)$.

For large B fields, giving rigidity $\mathcal{R} \gg 1$, simple z-bounce-averaged theory suffices to describe the separatrix-induced transport and wave-damping. The tilt-induced z-asymmetric error field $\delta\phi_a(r,z)$ has bounce averages values

$\delta\phi_L$ and $\delta\phi_R$ for left- and right-end trapped particles near the separatrix energy, with passing particles experiencing zero bounce-average error fields. The drift orbits for left- and right-end trapped trajectories are then offset radially by

$$\Delta r = \overline{\delta\phi_L} - \overline{\delta\phi_R} \Big/ \overline{\partial\Phi_e/\partial r}. \tag{1.2}$$

Random transitions between trapped and passing populations are caused by collisions (*c*); by drift rotation along the $\cos(m\theta)$ separatrix ruffles (*m*); and by temporal fluctuations in the separatrix energy (*t*). If the fraction of particles transitioned in a rotation period is η, then the radial diffusion coefficient is expected to be

$$D_r \sim \eta f_E \Delta r^2. \tag{1.3}$$

For collisions alone, conventional neoclassical ripple transport gives $\eta_c \equiv \Delta W_c F_M(\phi_{s0}) \propto \nu^{1/2} B^{1/2}$. Collisions limit the separatrix–induced "fracturing" of the velocity distribution to an energy width $\Delta W_c \sim T(\nu / f_E)^{1/2}$. In contrast, the ruffle η_m and temporal η_t processes will be seen to be independent of both ν and B.

With plasma rotation across a separatrix *ruffled* by $\Delta\phi_2$, a detailed analysis [11, 12] of transitions between the left and right trapping regions gives neoclassical diffusion coefficient

$$\begin{aligned} D_r(r) &= \tfrac{1}{4} F_M(\phi_{s0}) f_E \Delta r^2 \\ &\times \Delta W_c D_{cA} + \Delta\phi_2 D_{2A} \sin^2\alpha \ . \end{aligned} \tag{1.4}$$

Both the collisional bounce-Averaged transport coefficient D_{cA} and the $m = 2$ ruffle coefficient D_{2A} calculated in [12] as functions of the normalized ruffle strength $\Delta\phi_2 / \Delta W_c$ are shown in Fig. 2. The ruffle-induced transport coefficient D_{2A} is nearly independent of $\Delta\phi_2 / \Delta W_c$, giving $D_r \propto \Delta\phi_2$. In contrast, the collisional coefficient D_{cA} shows a fast decline as chaotic separatrix crossings become dominant and smooth out the collision-induced fractures of F_M.

In the case of perfectly aligned asymmetries ($\sin^2\alpha \approx 0$), ruffles may enable some suppression of collisional neoclassical ripple transport, until the bounce-resonant transport processes become dominant on their own.

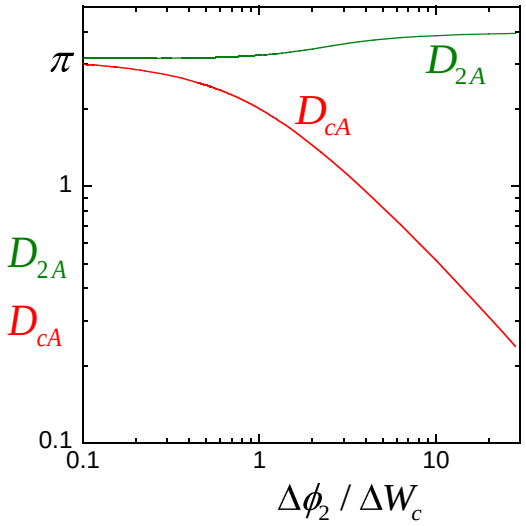

Figure 2. Calculated collisional D_{cA} and ruffle induced D_{2A} coefficients versus the normalized ruffle strength.

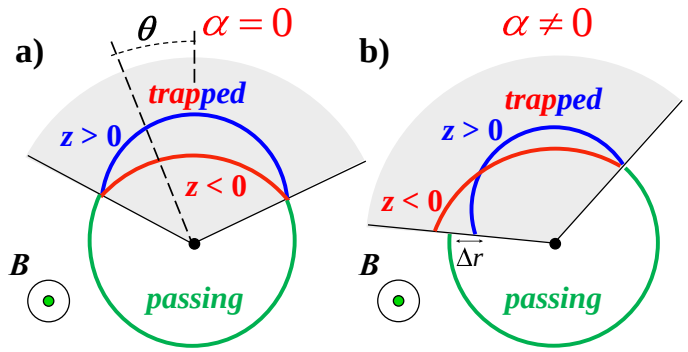

Figure 3. Sketch of split *E*×*B* drift orbits near the $m = 2$ ruffled separatrix. a) $\alpha = 0$. b) $\alpha \neq 0$. For the magnetic tilt asymmetry the trapped portions of the orbits are the partial circles shifted along the tilt direction.

Indeed, prior theory [7] considered only $\alpha = 0$ or π, in which case the phase-dependent part of the diffusion coefficient is exactly zero. The reason for this cancellation can be qualitatively understood from Fig.3a, which shows a sketch of split *E*×*B* drift orbits near the $m = 2$ ruffled separatrix. From the magnetic tilt asymmetry the trapped portions of the drift orbits are partial circles shifted along the tilt direction. If this direction coincides with the zero phase of separatrix ruffle, the left-right symmetry implies particles transit from trapped to passing and back at the same radius, so the drift orbit is closed and there is no net radial step.

However, when $\alpha \neq 0$ or π, the symmetry is broken and particle orbits are trapped and detrapped at different radii, leading to radial steps $\Delta r \neq 0$ (Fig.3b). Of course, for $\alpha = 0$ or π the diffusion does not completely vanish; collisional effects not kept in the above analysis yield finite diffusion consistent with the one obtained in [7]. Nevertheless, this perfect "stellarator symmetry" with respect to all global asymmetries is commonly assumed in stellarator optimization theory.

Figure 4 shows the predicted transition from predominantly collisional neoclassical diffusion to the chaotic regime (ruffle dominated, $D_r \propto \Delta\phi_2 D_{2A}$). For comparisons with the experiments, the effective transport coefficient D_* can be rather conveniently approximated as

$$\begin{aligned} D_* &\equiv \Delta W_c D_{cA} + \Delta\phi_2 D_{2A} \sin^2\alpha \\ &\approx 4(\Delta\phi_2 \sin^2\alpha + 0.88\Delta W_c e^{-\Delta\phi_2/0.88\Delta W_c}). \end{aligned} \tag{1.5}$$

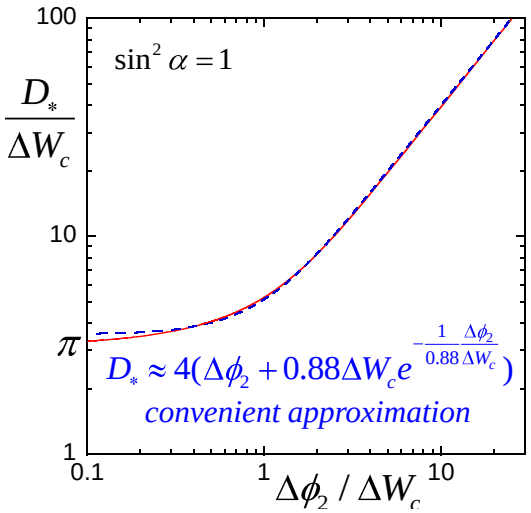

Figure 4. Combined neoclassical ripple transport coefficient D_* versus the normalized ruffle strength. The dashed line is the approximate form (1.5).

The full radial flux has both mobility and diffusive contributions, as

$$\Gamma_r = \mu \ \partial\Phi_e/\partial r \ - D_r \ \partial N_0/\partial r \ , \tag{1.6}$$

with $\mu = D_r N_0/T$ and $N_0 \equiv \int d_z n$. This flux definition implies $\Gamma_r \propto D_r$, and then connects it to the bulk expansion rate as

$$\nu_{<r^2>} = \int r dr\, r^2 \frac{1}{r}\frac{\partial}{\partial r} r\,\Gamma_r \Big/ \left\langle r^2 \right\rangle . \tag{1.7}$$

4. Experiments

Figure 5 shows the measured expansion rate $\nu_{<r^2>}$ as a function of the $m=2$ ruffle voltages ΔV_2 at the wall for the maximal transport alignment $\sin^2\alpha = 1$. It has essentially the same fitting function as the calculated one in Fig.4, giving the normalized "radially averaged" ruffle strength as $\left\langle \Delta\phi_2 / \Delta W_c \right\rangle_r \approx (4/3)\Delta V_2 / 1\mathrm{V}$. This is close to its estimated value. Thus, at $B = 6\,\mathrm{kG}$ and $\Delta V_2 = 3\mathrm{V}$, the effective ruffle width $\Delta\phi_2$ is approximately 4× the collisional width $(\Delta\phi_2 \approx 4\Delta W_c)$, and the transport rate has changed by a factor of 4× accordingly.

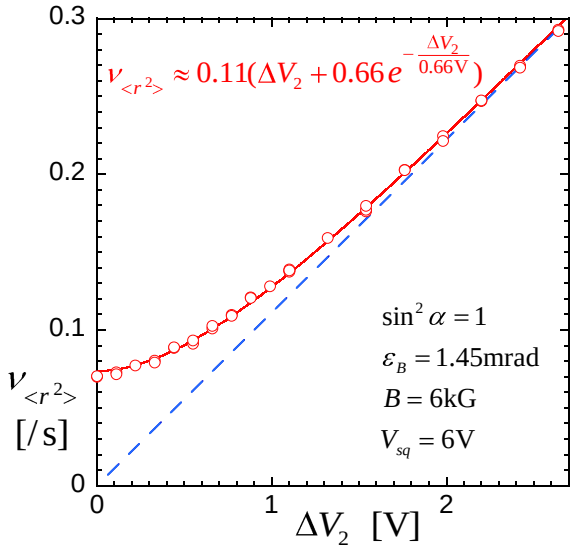

Figure 5. Measured expansion rate as a function of the ruffle voltage at the wall ΔV_2.

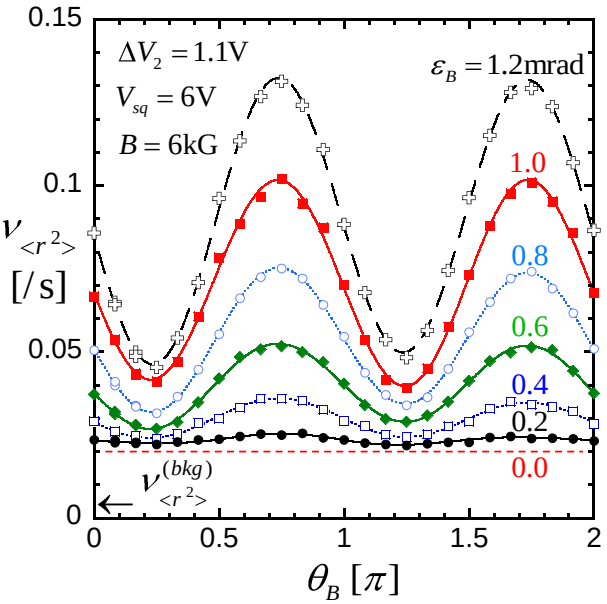

Figure 6. Measured transport rate $\nu_{<r^2>}$ at fixed $\Delta V_2 = 1.1\mathrm{V}$, showing chaotic part of neoclassical transport varying as $\varepsilon_B^2 \sin^2\alpha$, and α-independent collisional ripple transport.

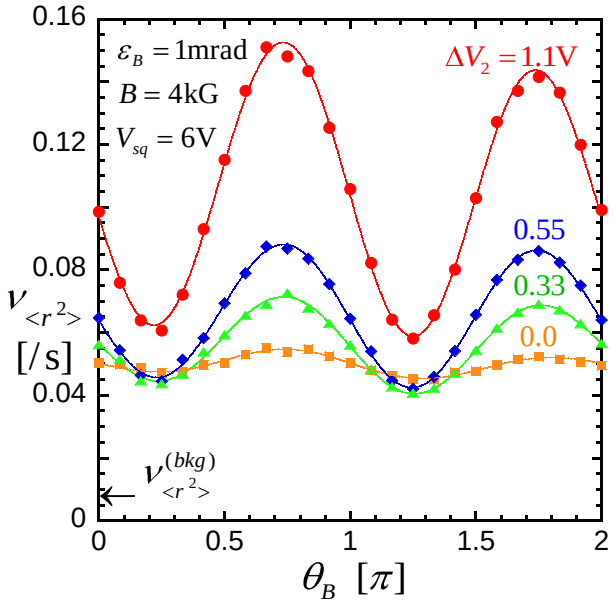

Figure 7. Measured transport rate $\nu_{<r^2>}$ at fixed $\varepsilon_B = 0.001$, showing chaotic part of neoclassical transport varying as $\Delta V_2 \sin^2\alpha$, and α-independent collisional ripple transport.

Figure 6 is a plot of measured expansion rate $\nu_{<r^2>}$ versus the magnetic tilt angle θ_B, for various tilt strengths ε_B at a fixed wall ruffle value $\Delta V_2 = 1.1\text{V}$. The ruffled-induced part shows an unambiguous $\varepsilon_B^2 \sin^2\alpha$ dependence on relative angle $\alpha = \theta_B - \theta_m$, (here, $\theta_2 \approx \pi/4$) with the magnitude proportional to ΔV_2. Separate data varying θ_2 in steps of $\pi/2$ verifies the dependence on relative angle α only.

Similarly, Figure 7 is a plot of measured expansion rate $\nu_{<r^2>}$ versus magnetic tilt orientation angle θ_B, for various applied wall ruffle strengths ΔV_2, now at the fixed tilt value $\varepsilon_B = 0.001$. Once again, the ruffled-induced part of the transport rate shows its unambiguous $\Delta V_2 \sin^2\alpha$ signature, but now with magnitude proportional to ε_B^2.

The distinctive $\varepsilon_B^2 \sin^2\alpha$ signature, together with separate control of ΔV_2 and ε_B, enables clear experimental identification of *z*-bounce-Averaged neoclassical transport processes separately from *z*-kinetic processes. We model the full transport rate as

$$\begin{aligned}\nu_{<r^2>} &= C_{cA}(\Delta V_2)\varepsilon_B^2 + C_{2A}\varepsilon_B^2 \Delta V_2 \sin^2\alpha \\ &+ C_{cK1}\varepsilon_B^2 + C_{cK2}\Delta V_2^2 + \nu^{(bkg)}_{<r^2>},\end{aligned} \tag{1.8}$$

where C_{cA} and C_{2A} represent the radial integrals of Eqn. (1.4); C_{cK1} and C_{cK1} represent collisional Kinetic (bounce-resonant) transport driven by ε_B^2 and ΔV_2^2 as *z*-dependent "error" fields [13-15]; and small $\nu^{(bkg)}_{<r^2>}$ arises from uncontrolled background tilts, separatrices, and omnipresent ruffles. Here, for dimensional simplicity, $\varepsilon_B \equiv \varepsilon_B / 1\text{mRad}$ and $\Delta V_2 \equiv \Delta V_2 / 1\text{Volt}$.

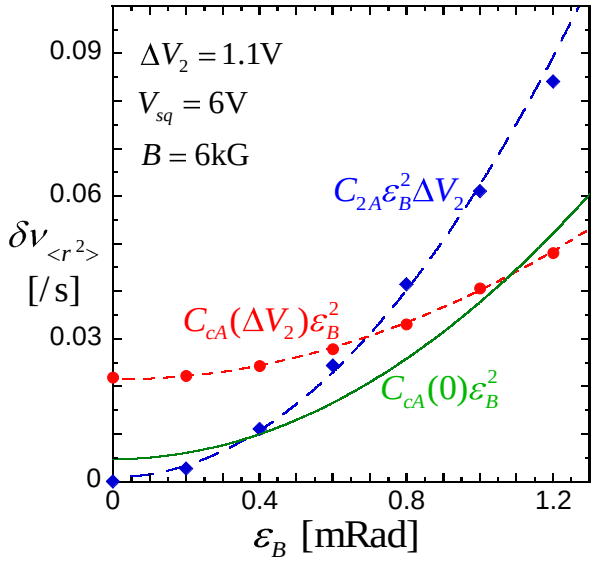

Figure 8. Measured ε_B^2 scalings for the C_{2A} and $C_{cA}(\Delta V_2)$ neoclassical ripple transport terms at $B = 6\,\text{kG}$. Every marker here (not shown for $C_{cA}(0)$) is the result of $(a + b\sin^2\alpha)$ fit like those shown in Fig. 6.

C_{2A} and $C_{cA}(\Delta V_2)$ are readily obtained from the $\sin^2\alpha$ dependences such as shown in Figs. 6 and 7; and varying ε_B gives the expected ε_B^2 scaling, as shown in Fig. 8. Data taken with $\Delta V_2 = 0$ defines $C_{cA}(0) \approx 0.033/\text{sec}$. Comparing $C_{cA}(0)$ to $C_{cA}(1.1\text{V}) \approx .019/\text{sec}$ and using the $D_{cA}(\Delta\phi_2/\Delta W_c)$ data from Fig. 2, one can get another estimate on the "radially averaged" ruffle strength, as $\langle \Delta\phi_2/\Delta W_c \rangle_r \approx (4/3)\Delta V_2/1\text{V}$; and this is consistent with the previous conclusion based on the results in Figs. 4 and 5.

Data taken with $\varepsilon_B = 0$ show a $\nu^{(bkg)}_{<r^2>}$ offset and a parabolic dependence on the applied ΔV_2, giving C_{cK2}. Varying ε_B then selects C_{cA} and C_{cK1}; these terms are distinguished by their *B*-scaling (discussed next), and by the fact that the *z*-antisymmetric bounce-averages in C_{cA} require the separatrix, whereas the kinetic C_{cK1} depends only weakly on the applied squeeze voltage. In Fig. 7, $C_{cK2}(4\,\text{kG}) \approx 0.03/\text{sec}$, giving elevated $\sin^2\alpha$ minima for large ΔV_2; the depressed minima for $\Delta V_2 = 0.33\text{V}$ are from ruffle-suppression of $D_{cA}(\Delta\phi_2/\Delta W_c)$ (see Fig. 2); and $\nu^{(bkg)}_{<r^2>} \approx 0.007/\text{sec}$.

Figure 9 shows the measured transport rate coefficients C_{2A}, C_{cA} and C_{cK1} versus magnetic field, with experimental scalings (dashed), compared to theory (solid lines). At high B, the measured chaotic and collisional separatrix transport processes agree closely with theory, scaling as B^{-1} and $B^{-1/2}$ respectively. Here the accuracy of comparison is limited by experimental temperature uncertainty, by sensitivity of calculations to the plasma edge density gradients, and by transport induced modification of $F_M(\phi_{s0})$. We note that prior transport scaling experiments have been confused by the presence of uncontrolled separatrices and ruffles, as well as by overlapping transport regimes [8].

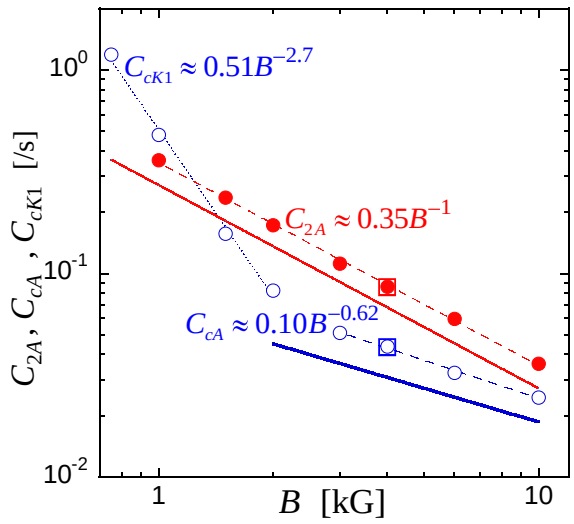

Figure 9. Measured transport rates C_i versus B at $V_{sq} = 6\,\mathrm{V}$ with empirical scalings. Solid lines are theory predictions.

5. Kinetic Effects

At low B, the kinetic (bounce-resonant) transport part, labeled as C_{cK1} in Fig. 9, is observed to depend strongly on field $(\propto B^{-2.7})$; but no simple power law is theoretically expected, since multiple bounce-rotation resonances become dominant. Then, the radial flux is dominated by long-time-correlated quasi-periodic orbits which initially show radial spreading proportional to time. At ultra low collisionality, when $\Delta W_c \ll \Delta\phi_m / \mathcal{R}$, particles retain information about many previous collisionless crossings of the ruffled separatrix. Using normalized ruffle strength $A_s \equiv 2\Delta\phi_2 / w$ (here $w = \Delta W_c \mathcal{R}^{-1/2}$ is the energy collisional spreading during one axial bounce at the separatrix energy) as a parameter we have done a numerical bounce-mapping of the mean radial particle flux versus rigidity. The calculated factor for the phase ($\sin^2\alpha$) independent part of the radial flux is shown in Fig. 10, including the transition from the bounce-averaged to the bounce-resonant regime. A numerical calculation gives the α–independent flux coefficient J_c versus rigidity $\mathcal{R}$, for 4 values of the normalized ruffle strength A_s. The "strong ruffle" curve scales as $2A_s / \mathcal{R}$ (i.e., as B^{-1}) in the high-rigidity regime $\mathcal{R} \gg A_s^{2/3}$, but shows strong resonant enhancement at small integer $\mathcal{R} \ll A_s^{2/3}$; and an estimate of their maxima gives $J_c \propto \mathcal{R}^{-2.5}$, in general correspondence to the $B^{-2.7}$ scaling observed for C_{cK1} at low B. At large $\mathcal{R}$, the $A_s = 32$ flux scales as B^{-1}, in correspondence with the C_{2A} and the bounce-averaged theory. The $A_s = 0$ curve scales as $B^{-1/2}$, in quantitative correspondence with "no ruffle" collisional neoclassical transport. Overall, this numerical mapping shows close correspondence both with analytical results for bounce-average case (collisional and chaotic) and with experimental scalings in the whole bounce-average and bounce-resonant domain.

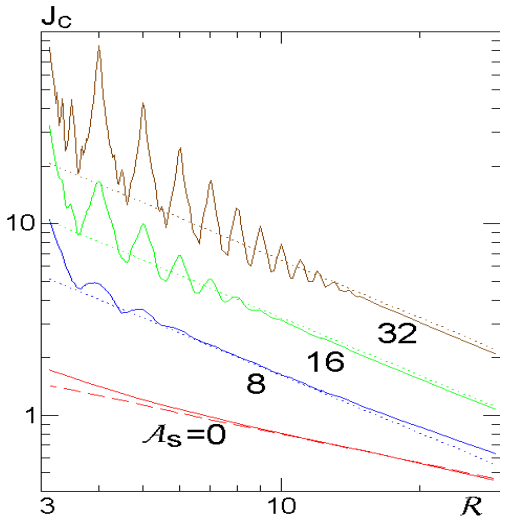

Figure 10. Numerically calculated α–independent dimensionless radial flux J_c versus rigidity $\mathcal{R}$ for indicated values of ruffle strength A_s. In the range $\mathcal{R} \ll A_s^{2/3}$ the curves have resonant spikes. The dotted lines are analytical results in the chaotic case, $J_c = 2A_s / \mathcal{R}$. The red dashed line $(A_s = 0)$ is analytical result in the collisional case, $J_c = (2\pi / \mathcal{R})^{1/2}$

6. Fluctuation-induced transport

Similar enhanced particle transport is observed when there are temporal variations in the separatrix energy. Figure 11 illustrates the immediate increase in radial expansion rate induced when white noise $(V_{RMS} = 0.2\,\mathrm{V},\ f_E < f < 20\,\mathrm{MHz})$ is applied to the θ-symmetric ripple (squeeze) ring, driving random (collisionless) separatrix crossings. The 3× increase in $(d/dt)\langle r^2 \rangle$ rate observed here is consistent with a collisional separatrix layer width $\Delta W_c \approx 0.07\,\mathrm{eV}$ fluctuating by $\Delta\phi(t) \approx 0.2\,\mathrm{eV}$. Presumably, any noise- or wave-induced fluctuations which change particle kinetic energies relative to the separatrix energy would be equally effective in enhancing neoclassical helical ripple transport.

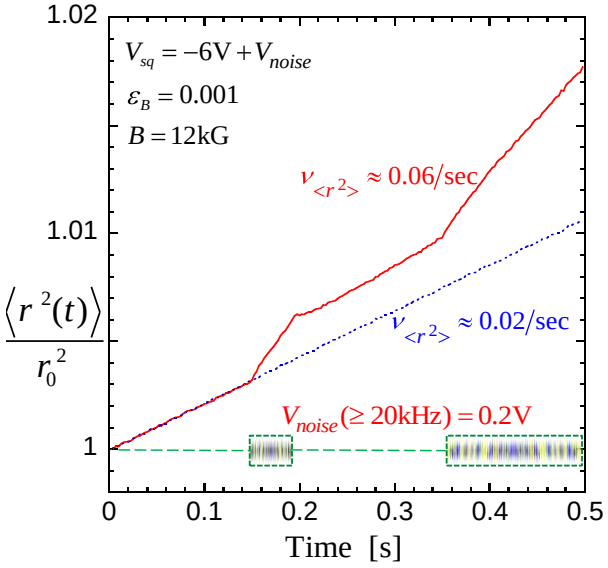

Figure 11. Enhanced transport rate during the two bursts of 0.2V (RMS) white noise $\Delta\phi(t)$) applied to an electrostatic ripple.

7. Low-collisionality enhancement

A summary of the different transport regimes is shown in Fig. 12, which sketches the radial diffusion coefficient versus collision frequency**.** We emphasize that this perspective is supported by quantitative experiments [Refs. 8-10 and Refs. therein], in agreement with detailed theory and targeted simulations [3,4,11,12]. This research enabled

identification of the different regimes characterized by collisional energy spreading ΔW_c, ruffle amplitude $\Delta\phi_m$, and fluctuation amplitude $\Delta\phi(t)$; and it clarified the connection to kinetic processes at low rigidity $\mathcal{R}$.

This broader perspective may aid in interpretation of numerical simulations developed for stellarator geometry [16] (Beidler et al. 2011), where multiple processes combine. Moreover, recent stellarator measurements [17] (Pedrosa et al. 2014) suggests that electric potential variations may occur even along field lines, and that drift-kinetic effects may be significant. These effects are necessarily considered in cylindrical (open) traps, but are often neglected in analysis of stellarators and tokamaks.

In Fig. 12, the $\nu^{1/2}$ and ν^1 lines (red) represent standard "superbanana" collisional transport, with the ν^1 regime predicted due to suppressed collisional transport from the presumed $\alpha = 0$ symmetry. This corresponds to the ruffle-induced reduction of D_{cA} in Fig. 2, with D_{2A} being presumed ineffective due to $\sin^2\alpha \approx 0$ in Eqn. 1.4.

Without the $\alpha = 0$ presumption of dynamically reversible drifts, transport due to ruffles (green) and due to temporal potential fluctuations (orange) may dominate at low ν. Both of these processes are essentially independent of ν. At ultra low (probably unphysically low) ν, nonlinear effects could limit these transport mechanisms.

Overall, our experiments, theory and computer simulations suggest that chaotic neoclassical transport due to ruffles or fluctuations scaling as ν^0 may well be dominant in regimes of low collisionality (Fig. 12). Thus, considerable work may be required to bring theory into correspondence with low-collisionality, separatrix-ruffled, fluctuating fusion plasmas.

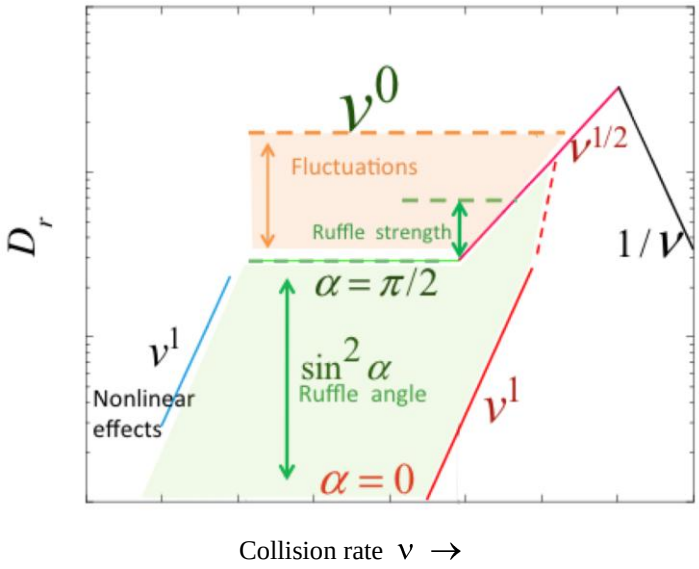

Figure 12. Low collisionality chaotic transport due to ruffles or due to temporal fluctuations may increase the diffusion rate well above its collisional predictions in ν^1 and $\nu^{1/2}$ regimes.

Most plasma confinement devices have trapping separatrices (ripples), arising from variations in magnetic field strength or external potentials. These separatrices are never perfectly symmetric, or perfectly aligned with other asymmetries. If the separatrix itself is asymmetric or temporally perturbed, the drifting particles collisionlessly change from trapped to passing and back, leading in the case of low collisionality $(\nu / f_E \ll 1)$ to enhanced asymmetric ripple transport $(\propto \nu^0 B^{-1})$ in comparison to the standard neoclassical ripple transport $(\propto \nu^{1/2} B^{-1/2})$. When the separatrix layer collisional width is less than its θ-asymmetry or temporal perturbations, this new loss mechanism becomes the dominant bulk transport process in our non-neutral plasma experiments, and it could have important implications for similar low collisionality regimes in other magnetic conferment experiments.

Acknowledgments

This work was supported by National Science Foundation Grants PHY-0903877 and PHY-0613740, and by Department of Energy Grant DE-SC0002451.

References

1. P. Helander, D.J. Sigmar. *Collisional Transport in Magnetized Plasmas*, Cambridge: “Cambridge University Press”, 2002.
2. M.N. Rosenbluth, D.W. Ross, D.P. Kostomarov. Stability regions of dissipative trapped-ion instability// *Nuclear Fusion*, 1972, v. 12, N1, p. 3-37.
3. T.J. Hilsabeck, T.M.O'Neil. Trapped-particle diocotron modes// *Physics of Plasmas*. 2003, v. 10, N9, p. 3492-3505.
4. D.H.E. Dubin. Theory and simulations of electrostatic field error transport// *Physics of Plasmas*. 2008, v. 15, N7, p. 072112-26.
5. T. Ohkawa, J.R. Gilleland, T. Tamano. Observation of neoclassical, intermediate, and Pfirsch-Schulter diffusion in the dc octople// *Physical Review Letters.* 1972, v. 28, N17, p. 1107-1111.
6. M.C. Zarnstorff, K. McGuire, et. al. Parallel electric resistivity in the TFTR tokamak// *Physics of Fluids B*. 1990, v. 2. N8, p. 1852-1857.
7. H.E. Mynick. Effect of collisionless detrapping on non-axisymmetric transport in a stellarator with radial electric field// *Physics of Fluids*. 1983, v. 26, N9, p. 2609-2615.
8. A.A. Kabantsev, C.F. Driscoll. Trapped-particle modes and asymmetry-induced transport in single-species plasmas// *Physical Review Letters*. 2002, v. 89, N24, p. 245001-4.
9. A.A. Kabantsev, T.M. O'Neil, Yu.A. Tsidulko, C.F. Driscoll. Resonant drift-wave coupling modified by non-linear separatrix dissipation// *Physical Review Letters*. 2008, v. 101, N6, p. 065002-4.
10. A.A. Kabantsev, C.F. Driscoll. Trapped-particle mediated collisional damping of nonaxisymmetric plasma waves// *Physical Review Letters*. 2006, v. 97, N9, p. 095001-4.
11. D.H.E. Dubin, C.F. Driscoll, Yu.A. Tsidulko. Neoclassical transport caused by collisionless scattering across an asymmetric separatrix// *Physical Review Letters*. 2010, v. 105, N18, p. 185003-4.
12. D.H.E. Dubin, Yu.A. Tsidulko. Neoclassical transport and plasma mode damping caused by collisionless scattering across an asymmetric separatrix// *Physics of Plasmas*. 2011, v. 18, N6, p. 062114-17.
13. D.L. Eggleston, T.M. O'Neil. Theory of asymmetry-induced transport in a non-neutral plasma// *Physics of Plasmas*. 1999, V. 6, N7, p. 2699-2704.
14. D.L. Eggleston, J.M. Williams. Magnetic field dependence of asymmetry-induced transport: a new approach// *Physics of Plasmas*. 2008, v. 15, N3, p. 032305-6.
15. E.P. Gilson, J. Fajans. Quadrupole-induced resonant-particle transport in pure electron plasma// *Physical Review Letters*. 2003, v. 90, N1, p. 015001-4.
16. C.D. Beidler, K. Allmaier, M.Yu. Isaev, S.V. Kasilov, W. Kernbichler, G.O. Leitold, H. Maaßberg, D.R. Mikkelsen, S. Murakami, M. Schmidt, D.A. Spong, V. Tribaldos and A. Wakasa. Benchmarking of the mono-energetic transport coefficients—results from the International Collaboration on Neoclassical Transport in Stellarators (ICNTS)// *Nuclear Fusion*. 2011, v. 51, N7, p. 076001-28.
17. M.A. Pedrosa, J.A. Alonso, J.M. García-Regaña, C. Hidalgo, J.L. Velasco, I. Calvo, C. Silva, P. Helander. Electrostatic potential variations along flux surfaces in stellarators// arXiv:1404.0932.